

# A Comparative Analysis of Near-Storm Environments for Tornadic and Nontornadic Significant-Hail Supercells using the Warn-on-Forecast System (WoFS)

Jerod W. Kaufman,<sup>a,b</sup> David A. Rahn,<sup>a</sup> Patrick C. Burke,<sup>c</sup> Montgomery L. Flora,<sup>e,c</sup> Corey K. Potvin,<sup>c,d</sup> and David B. Mecham<sup>a</sup>

<sup>a</sup> Department of Geography and Atmospheric Science, University of Kansas, Lawrence, Kansas

<sup>b</sup> NOAA/National Weather Service, Wichita, Kansas

<sup>c</sup> NOAA/OAR/National Severe Storms Laboratory, Norman, Oklahoma

<sup>d</sup> School of Meteorology, University of Oklahoma, Norman, Oklahoma

<sup>e</sup> Cooperative Institute for Severe and High-Impact Weather Research and Operations, University of Oklahoma, Norman, Oklahoma

*Corresponding author:* David A. Rahn, darahn@ku.edu

**Early Online Release:** This preliminary version has been accepted for publication in *Weather and Forecasting*, may be fully cited, and has been assigned DOI 10.1175/WAF-D-25-0016.1. The final typeset copyedited article will replace the EOR at the above DOI when it is published.

© 2025 American Meteorological Society. This is an Author Accepted Manuscript distributed under the terms of the default AMS reuse license. For information regarding reuse and general copyright information, consult the AMS Copyright Policy ([www.ametsoc.org/PUBSReuseLicenses](http://www.ametsoc.org/PUBSReuseLicenses)).

**ABSTRACT:** The National Severe Storm Laboratory's Warn-on-Forecast System (WoFS) is an ensemble of convection-allowing simulations designed for short-term (0–6 h) forecasting of severe weather, with the goal of helping the community move from a warn-on-detection to a warn-on-forecast paradigm. Although broader environmental conditions for severe weather in WoFS have been examined, no previous work has assessed meso-beta-scale environmental features adjacent to supercells that WoFS is able to resolve. A total of 41 supercells associated with local storm reports of either tornadoes rated at least EF1 or nontornadic significant hail (>51 mm diameter) are studied using WoFS simulations. The meso-beta-scale environments of tornadic and nontornadic significant-hail supercells are compared and contrasted using composite fields of salient parameters centered on the associated storm reports, and also by using back trajectories starting in the storm inflow region near the updraft at the time of the report. Composites reveal that WoFS simulates a noticeable pocket of high 0–500-m storm-relative helicity (SRH) that is significantly stronger and larger for tornadic than for nontornadic significant-hail supercells. Back trajectories also reveal environmental properties approaching the tornadic storms, such as consistently low lifting condensation levels and values of 0–500-m SRH that begin favorably and steadily increase.

**SIGNIFICANCE STATEMENT:** The earlier a severe weather warning is issued, the sooner people can act. Currently, warnings are based on weather radars or spotter reports while severe weather is occurring or imminent. To investigate the possibility of warning *well before* severe weather occurs, we examine 1-hour computer simulations from the Warn-on-Forecast System (WoFS) to identify environmental signals that separate tornadic supercells from supercells that produce significant hail but no tornadoes. Although other studies have examined broader environmental conditions, we focus on smaller-scale (10s of km) features in the near-storm environment. WoFS forecasts exhibit various small-scale discriminating features, such as nearby pockets of enhanced low-level wind shear to the inflow side of tornadic supercells, which offer promising markers for early warnings.

## 1. Introduction

The National Weather Service assesses the potential for severe weather days before the anticipated event over broad areas. This forecast is communicated through the Storm Prediction Center's convective outlooks, and the forecast is refined leading up to the time of the event. Warnings at the storm scale are issued in real time based primarily on radar signatures, but also with reports from trained spotters. Despite improvements in the accuracy of National Weather Service warnings over the past few decades, the average lead time for tornadoes decreased from 18.8 min from 1986 to 2011 to 15.6 min from 2012 to 2016 (Brooks and Correia 2018). Although this occurred due to "an apparent increased emphasis on reducing false alarms," it further resulted in a decreased probability of tornado detection (Brooks and Correia 2018). With an overarching goal to address these conflicting priorities, the aim of the Warn-on-Forecast project is to help facilitate "a new warning paradigm beyond warn-on-detection" that aims to further increase the lead time in warning and detection for events such as tornadoes (Stensrud et al. 2009, 2013; Heinselman et al. 2024). The Warn-on-Forecast System (WoFS) is designed to help forecasters improve the warning lead time for convective storms (Stensrud et al. 2009). Early WoFS prototypes demonstrated their effectiveness in producing short-term forecasts of hazards such as hail (Snook et al. 2016), heavy rain (Yussouf et al. 2016; Wilson et al. 2023; Burke et al. 2024), and tornadoes (Snook et al. 2012; Wheatley et al. 2015; Burke et al. 2022; Heinselman et al. 2024).

Based on the Weather Research and Forecast modeling system (Skamarock et al. 2019), WoFS is an ensemble of convective-allowing models (CAMs) developed by the Warn-on-Forecast project

at the National Severe Storms Laboratory. Many advances have occurred in forecasting the timing and location of storms since the initial conceptualization and development of CAMs (Done et al. 2004; Wilson et al. 2019). WoFS uses a 36-member analysis ensemble that assimilates the latest observations, including radar and satellite data, at 15-min intervals and produces a forecast ensemble with 18 members that is initialized at 30-min intervals. This ensemble of short-term CAMs is designed to provide additional guidance along the watch-to-warning timeline (0-6 h) and can be used to help anticipate if a particular storm will become severe before severe weather appears in radar data signatures or is directly reported by spotters.

Although the grid spacing of operational CAMs does not explicitly resolve all features and hazards that occur within thunderstorms, they still provide improved forecasts relative to larger-scale models (Kain et al. 2010). The horizontal grid spacing in WoFS is 3 km, similar to many current operational models such as the High Resolution Rapid Refresh (Benjamin et al. 2019; Dowell et al. 2022). Simulations with 1-km grid spacing, which are not yet viable for real-time operations due to the long computational times, perform better than simulations run with 3-km grid spacing (Miller et al. 2022; Kerr et al. 2023, 2025). However, the 3-km grids still provide relevant and useful information to guide forecasters in their decision making (Adlerman and Droege 2002; Bryan et al. 2003; Potvin and Flora 2015). Verification efforts using data from the Multi-Radar Multi-Sensor system demonstrated that WoFS can successfully capture salient features such as reflectivity and rotation (Skinner et al. 2018; Jones et al. 2020; Guerra et al. 2022). For operational purposes, CAMs and CAM ensembles such as WoFS need to run at a resolution fine enough to resolve the features of convective storms while also respecting the computational limits and delivery timelines such models are expected to meet in an operational setting.

WoFS provides probabilistic representations of many pertinent environmental parameters and a deterministic (e.g., individual member composite reflectivity) or quasi-deterministic (e.g., probability matched mean) representation of storm objects. These predictions can help forecasters anticipate situations that have an increased likelihood of a severe event and alert the general public of severe weather hazards (Lawson et al. 2018).

Since Smith et al. (2012) note that more than 95% of EF3 or greater tornadoes and significant hail events were associated with supercells, the focus here is on supercells and their surrounding environment, as represented by WoFS. Furthermore, tornadoes associated with right-moving su-

percells make up 89.1% of deadly tornadoes and 95.6% of all tornado deaths from 2003 to 2017 (Anderson-Frey and Brooks 2019). Based on the processes important for supercell-related severe weather (e.g., mesocyclogenesis and supercell tornadogenesis), there are several key environmental parameters that are used to anticipate environments that are likely to produce supercells and severe weather. Fundamentally, there must be sufficient instability to produce convective overturning, which is typically quantified by convective available potential energy (CAPE). This instability should (but does not always) coincide with minimal values of convective inhibition (CIN). Deep layer (0–6 km) shear must be of a sufficient magnitude per a given CAPE to allow for development and maintenance of a rotating updraft on time scales greater than that of a single updraft pulse or parcel. The deep layer shear reduces downdraft interference on the updraft, while lower-level wind shear creates horizontal vortex tubes that can be tilted into the vertical and then strengthened by stretching in the updraft. This process represents mesocyclogenesis and supercell-genesis, and its potential is often quantified by environmental storm-relative helicity (SRH) calculated in the 0–3 km layer (Davies-Jones et al. 1990; Droege et al. 1993; Markowski and Richardson 2010).

Shear and SRH within lower levels (e.g., 0–500 m and 0–1 km) have been shown to be key in discriminating between tornadic and nontornadic environments as they describe the potential for near-surface horizontal vorticity to be tilted by the updraft below the LFC (Coffer et al. 2019). Several mechanisms for supercell tornadogenesis are possible, but there are challenges to observing or simulating compelling evidence that clearly favors one over the other (Fischer et al. 2024). Conceptual models include those in Davies-Jones (2015), Orf et al. (2017), and Markowski (2024), with no evidence existing at present to rule out any of these proposed mechanisms, nor any indication that all tornadogenesis is associated with the same mechanism. Nevertheless, it is important to stress that regardless of the specific tornadogenesis conceptual model, the same underlying environmental parameters allow some degree of discrimination between tornadic and nontornadic supercell environments (e.g., a low lifting condensation level (LCL) and strong low-level shear associated with tornadic supercells), however there can be considerable overlap of environmental parameters (Johns et al. 1993; Grams et al. 2012).

Broad climatologies of severe weather events have characterized environmental parameters (Grams et al. 2012) including their spatial statistics (Smith et al. 2012). An increasing number of studies apply machine learning to help predict severe weather as reviewed in McGovern

et al. (2023). Many of these applications leverage ample reanalysis data at larger scales, such as Gensini et al. (2021) that used the 31-km ERA5 reanalysis to extract profiles 60–119 minutes before the storm report. Flora et al. (2021) used WoFS output with machine learning algorithms to help discriminate between severe weather hazards. They concluded that an end-to-end automated machine learning system is nearly impossible and proposed that human forecasters will continue to add value to machine learning forecasts of severe weather for the foreseeable future.

To complement these approaches, there is a need to examine case-based severe weather events using WoFS with verified storm reports and to use an approach that leverages the high spatial and temporal resolution of WoFS for resolving meso-beta-scale environmental features. The importance of the mesoscale patterns of these parameters is well recognized. Brooks and Doswell (1994) pointed out that relying on a single sounding near the storm is problematic because it can lead to ‘a great deal of concern for how to interpret the observations’ and noted large gradients in the mesoscale fields of CAPE and helicity from a numerical simulation.

The risk of using a single sounding to represent the mesoscale environment is also emphasized in Parker (2014). They use 134 soundings to investigate differences between seven tornadic supercells and five nontornadic supercells. Spatial composites of the standard metrics revealed clear differences with notably more favorable metrics in the far field for tornadic supercells. Nearest the storm, the nontornadic supercells have metrics that approach those of the tornadic supercells, suggesting that these are enhanced by the storm itself rather than associated with background conditions. Coniglio and Parker (2020) analyze hundreds of soundings taken close to supercells over the past 25 years. Among many findings, they highlight that tornadic supercells have higher 0–3 km SRH than nontornadic supercells with the largest differences concentrated in a region 90° to the right of storm motion. Although a possible explanation is that this region is a result of storm feedback, they suggest that there is a real difference in the background environmental SRH because there is greater heterogeneity in the tornadic subset than in the nontornadic subset.

The storm-induced effects on the near-storm environment have been investigated through various pathways. For instance, the radiative influence of cirrus anvils on the environment near the storm is investigated in Markowski et al. (1998), Frame and Markowski (2013), and Nowotarski and Markowski (2016). Other factors such as cell mergers and boundary interactions modify the near-storm environment and may influence tornadogenesis (e.g., Lee et al. 2006; Fischer and Dahl

TABLE 1. The list of parameters, levels examined, and parcel types used in this study, which includes mixed layer (ML), most unstable (MU), and surface-based (SB) parcels.

Parameter	Type/Heights
Convective Available Potential Energy (CAPE)	ML, MU, SB
Convective Inhibition (CIN)	ML, MU, SB
Lifting Condensation Level (LCL)	ML, MU, SB
Level of Free Convection (LFC)	ML, MU, SB
Storm-Relative Helicity (SRH)	0-500 m, 0-1 km, 0-3 km
Vertical Wind Shear	0-1 km, 0-3 km, 0-6 km
Significant Tornado Parameter (STP)	Fixed-Layer, 0-500 m SRH
Supercell Composite Parameter (SCP)	N/A

2023; Nixon et al. 2024). Given the complex nature of these interactions and the large diversity of real-world scenarios, there is still uncertainty regarding these aspects.

Real-world cases are routinely studied in WoFS. Much of the work examines storm objects in WoFS (e.g., Skinner et al. 2018; Britt et al. 2020; Guerra et al. 2022), but there has been less work that examines the meso-beta scale environment in WoFS outside of Potvin et al. (2020). Lindley et al. (2023) demonstrated WoFS ability to resolve fire-effective mesoscale weather features during southern Great Plains wildfire outbreaks, but no work has been published on similar features related to severe weather. This work seeks to address that gap by examining relevant features of the environmental fields associated with severe weather using WoFS and to understand what the spatial characteristics of these features are and how they differ between tornadic and nontornadic significant-hail supercells in WoFS.

The objectives here are to build on previous work by developing methods for identifying and extracting information on storms within WoFS that are associated with reported tornadoes or significant-hail events. Then, we characterize the environments of these groups and also quantify the differences as they evolve during the time leading up to the event. The results of this work are expected to help the community better incorporate the WoFS information into an operational setting.

## 2. Data

The National Severe Storms Laboratory provided archived model output from the WoFS project spanning 2017-2023. Given the high computing demand of running an ensemble of CAMs, WoFS

is run only on select days and over specific regional domains that typically correspond to enhanced or greater risk categories in the Storm Prediction Center (SPC) Day 1 Convective Outlook. The WoFS collection, therefore, excludes many lower risk days and locations that may also produce tornadoes or significant hail (Lawson et al. 2018). Additionally, over the period of interest, WoFS runs were performed from 1700 to 0300 UTC, so the data examined in this work did not include nocturnal or early morning storms. Table 1 lists the environmental parameters extracted from the three-dimensional fields of WoFS, which include standard metrics used to diagnose severe weather.

Storm reports are retrieved from the Local Storm Report database hosted by the National Centers for Environmental Information. These reports use the Enhanced-Fujita (EF) scale for tornado damage classification similar to Marshall et al. (2004). To determine which cases are included in the analysis, environments producing tornadoes rated EF1 and above and hail at least 51 mm in diameter are selected. By not including the EF0 classification, this removes tornadoes that generally occur in the presence of weaker mesocyclones and non-supercell storm modes. Storms with hail above 51 mm in diameter are considered ‘significant’ for this study, which is consistent with definitions at the SPC and in other products such as the Significant Hail Parameter. In cases where both an EF1+ tornado and significant hail occur, the event is classified as a tornado event.

### 3. Methods

#### a. *Storm classification and matching*

For days that have any reports of EF1+ tornadoes or nontornadic significant hail, the storm objects in all 18 WoFS ensemble members are classified following the algorithm developed by Potvin et al. (2022). Locations within each member are binarily classified as either containing a supercell or not. The criteria for the likely presence of a supercell are a model reflectivity that exceeds 43 dBZ and a 2-5 km updraft helicity that exceeds  $50 \text{ m}^2 \text{ s}^{-2}$ . The reflectivity threshold ensures that the model-identified storm contains an intense updraft, and the updraft helicity value is chosen because it represents the 99.95<sup>th</sup> percentile for mid-level updraft rotation in WoFS (Potvin et al. 2022). The exceedance of this threshold indicates substantial rotation within the identified object. Spatial characteristics of the identified object including eccentricity, solidity, and length of each identified storm object are then used to determine whether they fall under additional categories such as quasi-linear convective system (QLCS), supercell cluster, ordinary, and other.

The Neighborhood Maximum Ensemble Probability (NMEP) generally serves as “the likelihood of event occurrence anywhere within [a] coarse grid box” in ensemble forecast output (Schwartz and Sobash 2017). The supercell NMEP that is above 0.22 serves as a guide for the algorithm to find the center of potential supercells from the ensemble. This probability threshold allows for a focus on supercell-probable scenarios while also allowing for pseudo-supercell modes (e.g., mesocyclonic QLCS) to be preliminarily examined. This somewhat low probability also allows for the examination of low-probability supercells in the model that verified as supercells in reality. Furthermore, while not officially tested or grounded in previous research, the threshold was internally noted within the WoFS research group to be a good lower-end value for confidence regarding a model-identified supercell. However, most events had NMEP values clustered in the 0.33-0.56 range.

Next, reports of EF1+ tornadoes and nontornadic significant hail were matched to supercells in WoFS. First, to separate storms that had only significant hail from storms that had tornadoes, the significant hail reports that occur within 2 h and 100 km of any tornado report are removed. The 2 h and 100 km criteria are also used to constrain the search for the local storm report that is closest to a supercell in WoFS. These criteria are selected to minimize the chances of sampling a storm more than once. Previous studies (Grams et al. 2012) did this on a much larger scale (6 h and 300 km), but did so in an effort to eliminate the chances of oversampling broad environmental characteristics. These thresholds are lowered here because WoFS is able to capture finer storm details at its temporal resolution (5 min) than the RUC model used in the Grams study (1 h). WoFS is only run on select days over specific regional domains where the convective outlook has enhanced or greater risk categories. At these adjusted criteria, an adequate sample size of tornado (15) and significant-hail (26) cases is created. More information on specific event types, years, and locations is found in Tables 2-3 and Figure 1. Most events take place in the Great Plains from Texas to Nebraska and are mainly in May. As Coffer et al. (2019) point out, there can be large differences in the environmental parameters from one region to another, so results from one region or time may not be applicable to others. Forecast skill can also be biased from sampling (Coniglio and Thompson 2024), so it is important to note that results here may vary from other regions and times of year.

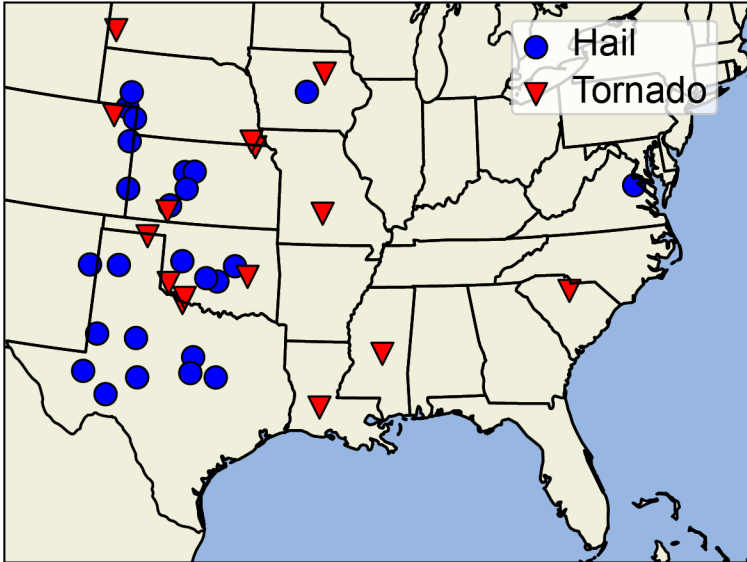


FIG. 1. The locations of tornado (red) and significant-hail (blue) reports.

The modest sample size is unlikely to fully represent the broad distribution of environments that are associated with nontornadic significant-hail and tornadic supercell environments. Additionally, the high concentration of reports located within the Central and Southern Plains as noted in Figure 1 may result in data that is unrepresentative of other regions covered by WoFS. However, a balance is sought between practical limitations, objectivity, maximizing the number of events, and removing dubious cases with the goal of providing more guidance for operational WoFS users. Even with this limited number of events, the results show promising trends within the WoFS parameters that indicate operationally relevant spatial and temporal results for short-term forecasts.

The classification algorithm used here serves as a fairly reliable objective method for classifying storm modes, and the classification was also manually inspected. However, it should be noted that the method can still misidentify confirmed supercells as ordinary storms. Sensitivity to thresholds was investigated, but only a few more cases were added for reasonable ranges of the thresholds. These ‘marginal’ supercells that are just below the chosen thresholds are not included to avoid being too permissive, but future work could use relaxed criteria to increase the sample size.

#### *b. Storm diagnostics*

Several approaches may be used to capture the environmental differences within WoFS between tornadic and significant-hail supercells. In the first method, which is the same method applied to

TABLE 2. Dates and locations for the tornadic supercells.

<b>Tornadic Supercells (15)</b>	
Date	Nearest Municipality
May 16, 2017	Minneola, KS
May 18, 2017	Harrold, TX
May 19, 2017	Dustin, OK
May 27, 2017	Lebanon, MO
May 2, 2018	Loveland, OK
May 20, 2019	Mangum, OK
May 22, 2019	Bern, KS
May 5, 2020	Great Falls, SC
May 8, 2020	Mamou, LA
May 4, 2021	Lena, MS
May 23, 2021	Sterling, CO
May 23, 2021	Sanator, SD
July 14, 2021	Shell Rock, IA
May 12, 2023	Pawnee City, NE
June 15, 2023	Perryton, TX

TABLE 3. Dates and locations for the significant-hail supercells.

<b>Significant-Hail Supercells (26)</b>			
Date	Nearest Municipality	Date	Nearest Municipality
May 25, 2017	Idalia, CO	May 26, 2021	Hays, KS
May 1, 2018	Nevada, IA	May 26, 2021	Oshkosh, NE
May 29, 2018	Ford, KS	May 27, 2021	Paden, OK
May 29, 2018	Ashton, KS	May 24, 2022	Knickerbocker, TX
May 3, 2019	Coyanosa, TX	May 31, 2022	Butler, OK
May 7, 2019	Gentry, TX	April 19, 2023	Chickasha, OK
May 7, 2019	Seminole, TX	April 26, 2023	Waco, TX
May 17, 2019	Sedgwick, CO	April 28, 2023	Shive, TX
May 4, 2020	Purcell, OK	May 9, 2023	Larned, KS
May 21, 2020	Coolidge, KS	May 10, 2023	Amherst, CO
May 10, 2021	Stephenville, TX	May 24, 2023	San Jon, NM
May 17, 2021	Snyder, TX	June 2, 2023	Terrell County, TX
May 26, 2021	Hays, KS	August 7, 2023	Hicks Mill, VA

the WoFS fields in Potvin et al. (2020), spatial composites of parameter fields are constructed by centering the domain on the WoFS convection associated with the nearby report, and at the closest model time within 15 min prior to the report. Using these domains, the probability matched mean (PMM, Ebert 2001) of each grid cell across all cases at the time of the report is created. Using

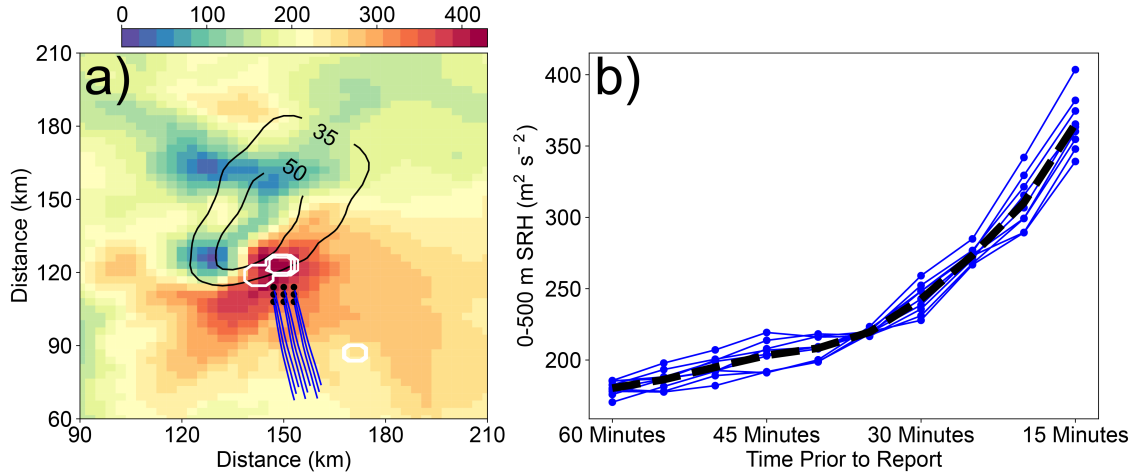


FIG. 2. Example of the 1-hr back trajectory method showing the (a) 0-500 m SRH (colors,  $\text{m}^2 \text{s}^{-2}$ ), model PMM reflectivity (black contours, dBZ), ‘parcel’ clusters (blue lines), and reported tornado (white circles), and (b) the time series of the 0-500 m SRH ( $\text{m}^2 \text{s}^{-2}$ ) for each parcel (blue) and the mean (black dashed).

the PMM allows for the preservation of each parameter’s probability density function, which is preferred over calculating a pure mean or median that is too easily swayed by outliers and overall smoothing of small-scale features.

While PMM composites provide a good depiction of the typical near-storm environment, different storm orientations and directions of the low-level inflow may blur the composites. The composites also do not easily convey information on the full distribution of the environmental parameters such as skewness. A second, complementary method calculates back trajectories starting at grid points within the inflow region of each storm just prior to the report. When going to this level of detail to examine environmental parameters in the vicinity of a storm, other issues may occur. Past studies have been cautious about examining near-storm environments because they are ‘contaminated’ by ongoing convection (e.g., Potvin et al. 2010; Grams et al. 2012). However, since the point of this work is to examine high-resolution spatial data in a CAM ensemble, these concerns are outweighed by the advantages of detecting differences on the meso-beta scale that could help identify supercells with more potential to produce tornadoes.

Instead of using a single point for the back trajectory analysis, a cluster of nine back trajectories are initialized over a  $3 \times 3$  square grid at the model grid points. The center of the grid is manually placed in a storm’s inflow region, no further than 30 km (10 grid points) away from the main

updraft (Fig. 2). Given that these are placed by hand, there is a certain level of subjectivity that could introduce possible bias from the placement of the parcels that may impact the along-parcel results. However, we endeavored to select as unbiased locations as possible. Furthermore, a grid of parcels is used to help diminish the sensitivity of the outcome to a single parcel choice, as the average results from a cluster of parcels should be more representative. Choosing different initial parcel locations would not substantially alter the values of the thermodynamic parameters since their gradients in the selected cases are not very large. However, the values of SRH, for example, could exhibit larger sensitivities to parcel choice given the larger SRH gradients seen in WoFS for these cases.

Each parcel's back trajectory is calculated at 5-min intervals, which are interpreted from the 15-minute output, back to 60 min prior to the storm report using a standard predictor–corrector approach:

$$P(t - \Delta t) = P(t) - \frac{1}{2}[V(P(t)) + V(P'(t - \Delta t))] \Delta t, \quad (1)$$

where  $t$  is the initial time,  $\Delta t$  is the time step (5 min), and  $P(t - \Delta t)$  is the final calculated position.  $V(P(t))$  is the velocity at the initial position, and  $V(P'(t - \Delta t))$  is the velocity at position  $P'$  previously calculated from a predictor step  $P'(t - \Delta t) = P(t) - V(P(t))\Delta t$ . The 0–1-km mean wind is used to represent the low-level inflow, and it is assumed that the inflow prior to being ingested into the storm has relatively small vertical motions compared to the horizontal wind. The position of each parcel at each time step is calculated to an exact location (not to a model grid point), and the corresponding wind at that location is bilinearly interpolated from the surrounding grid points.

Values for the suite of parameters listed in Table 1 are extracted at each time along the parcel's back trajectory by bilinearly interpolating from model grid points to the location of the back trajectory. An example of this method is illustrated in Fig. 2 using the 0–500 m SRH of a tornado-producing storm. Note the strong gradient in the vicinity of the convection, which corresponds to a large increase of SRH as the parcel approaches the time and place of the convection. The distribution of 0–500 m SRH for each parcel is relatively tight and tends to cluster about the mean value. Also, we note that Bunkers motion is used to find the SRH at each grid point.

To determine statistically significant differences between tornadic and nontornadic significant-hail supercells, a bootstrap hypothesis test (random resampling with replacement 1000 times) is used for the PMM composites and along the back trajectories with  $\alpha = 0.05$ .

The significant tornado parameter (STP) and the supercell composite parameter (SCP) combine convective parameters known to be conducive to such threats to create a single summary parameter of the pre-storm environment. The STP serves as a proxy for significant (EF2 or greater) tornado potential and combines the effects of mixed layer CAPE, CIN, and LCL alongside 0–1-km SRH and 0–6-km bulk wind difference into a single value. Environments containing values of STP greater than 1 have been shown to be conducive to significant tornadoes (Thompson et al. 2003, 2012). A later rendition of this parameter places greater importance on lower-level helicity by replacing the 0–1-km SRH with the 0–500-m SRH (Coffer et al. 2019). The fixed-layer bulk wind difference is also replaced with that of the effective layer, which is defined by a layer of CAPE exceeding  $100 \text{ J kg}^{-1}$  and CIN below  $250 \text{ J kg}^{-1}$ , and it has been shown to be the layer most likely to serve as the inflow for storms (Thompson et al. 2007). This alternative (hereafter 500STP) to the fixed-layer STP (hereafter FSTP) has been shown to be an even better discriminator between tornadic and nontornadic supercells (Coffer et al. 2019). The 500STP and FSTP contrast with the SCP (Thompson et al. 2002), which examines muCAPE alongside effective-layer SRH and bulk wind difference. Higher values of SCP are associated with right-moving supercells and estimate the likelihood of supercell development in a given environment. These composite summary parameters incorporate different aspects of an environment that are necessary for supercells and supercell tornadoes to develop.

## 4. Results

### a. Composites

#### 1) PRIMARY PARAMETERS

Differences between tornadic and nontornadic significant-hail supercells become readily apparent in the composites (Figs. 3–5). The muCAPE composites for both types of severe weather depict an environment with muCAPE above  $2000 \text{ J kg}^{-1}$  (Fig. 3). The greatest magnitudes are southeast of the storm center, which corresponds to the typical direction of inflow. WoFS routinely simulates high muCAPE in the vicinity ( $\sim 100 \text{ km}$ ) of the convection with differences between the tornadic and nontornadic significant-hail supercells up to  $1000 \text{ J kg}^{-1}$  mainly concentrated in the inflow region. The spatial distributions are similar, but the differences in magnitude suggest that tornadic environments are characterized by higher muCAPE on average. However, the distributions of

muCAPE and many other parameters (see section 4b and supplemental figures) exhibit substantial overlap between tornadic and nontornadic significant-hail supercells, which is consistent with earlier work that established the minimal discriminatory power of CAPE (Grams et al. 2012). For instance, there are higher values of muCAPE for tornadic cases west and southwest of the supercell, but the result is not significant for much of the area due to the large overlap.

One particular feature of note lies in the differences in the shape and size of the reflectivity contours (35 and 50 dBZ, respectively, in Figs. 3-5). Although the different sample sizes of the two events can slightly influence the results, the reflectivity contours associated with the tornadic supercells cover a greater extent than the nontornadic significant-hail supercells. Also, the larger 50-dBZ reflectivity core of the tornadic supercells exhibits a more concave shape than the more elliptical core in the hail supercells, which suggests precipitation wrapping around a weak echo region, at least for this sample of supercells which draws primarily from the Great Plains (Fig. 1).

The muLCL for both tornadic and nontornadic significant-hail supercells (Fig. 3d-f) follows the same general spatial pattern with muLCLs highest toward the southwest of the domain and decreasing toward the northeast (Fig. 3d-f). However, the muLCL is substantially lower for the tornadic events by about 500 m with the lowest heights occurring in the immediate vicinity of the storm. These minimum values extend 100 km towards the southeast, suggesting that not only does the surrounding environment exhibit a low muLCL, but WoFS also indicates a much lower muLCL throughout the entire region of the low-level inflow. This feature is consistent with past work that suggests the LCL plays a key role in discriminating between tornadic and nontornadic environments (Thompson et al. 2010, 2004). An environment with lower cloud bases (LCL) is favorable for enhanced tornadogenesis processes near the surface (low-level tilting, stretching, associated dynamic vertical perturbation pressure gradient force, and other related processes). With higher LCLs, tornadogenesis is less likely, but this does not necessarily inhibit a storm's ability to generate a strong enough mesocyclone and updraft that can produce significant hail. Therefore, this finding is physically consistent with processes occurring near supercells and confirms that WoFS is able to capture the magnitudes and spatial distributions of these parameters even when composited. Furthermore, the features depicted by the composites were also present when each case was examined individually.

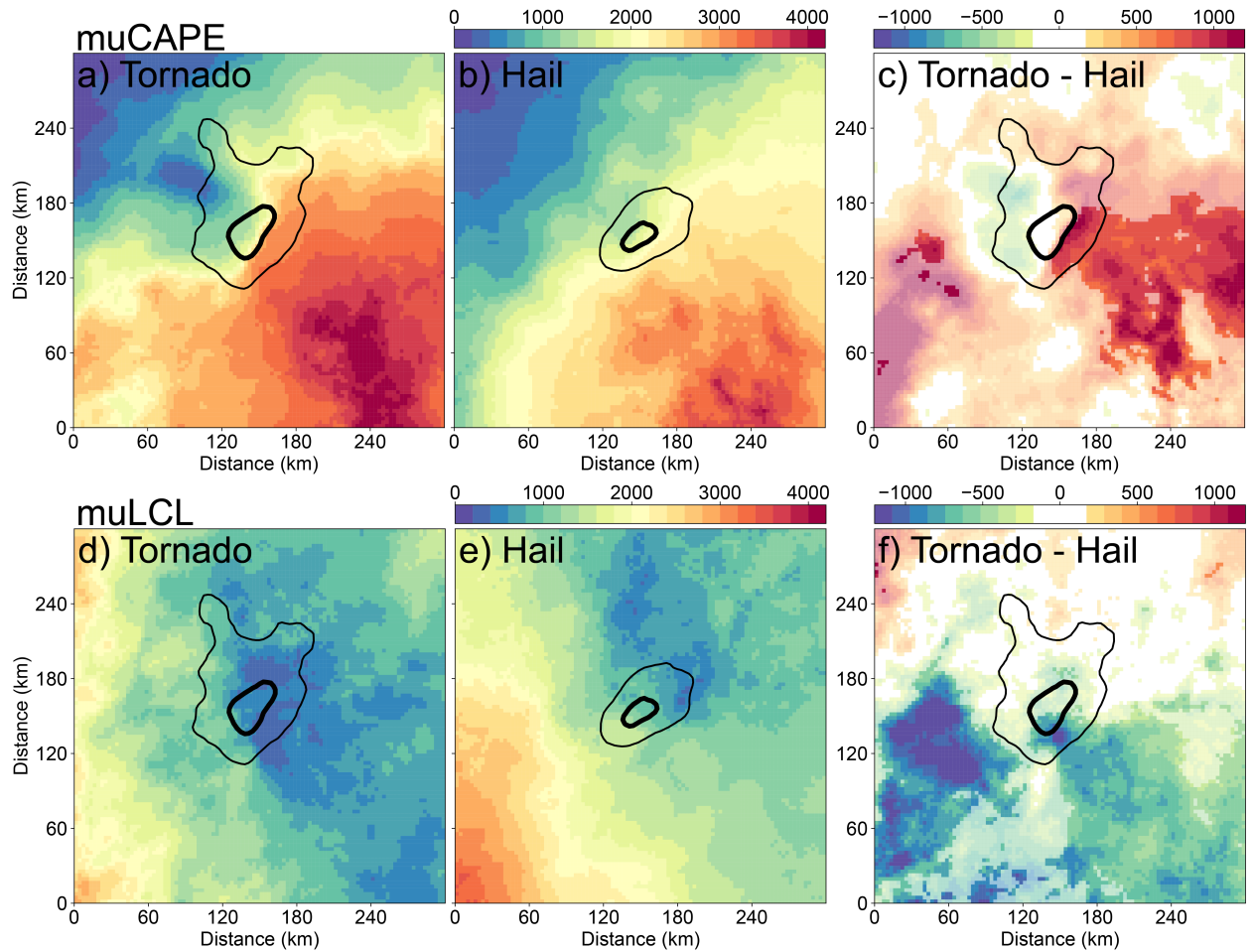


FIG. 3. PMM composites at the time of the report showing the muCAPE (colors,  $J \text{ kg}^{-1}$ ) for (a) tornadic supercells, (b) nontornadic significant-hail supercells, and (c) their differences (tornadic minus nontornadic significant-hail, insignificant differences are transparent), and the muLCL (colors, m) for (d) tornadic supercells, (e) nontornadic significant-hail supercells, and (f) their differences (tornadic minus nontornadic significant-hail, insignificant differences are transparent). Reflectivity is contoured at 35 dBZ (thin) and 50 dBZ (thick). The reflectivity of the tornadic cells is used for reference in the difference plots.

Differences between the tornadic and nontornadic significant-hail supercells are fairly pronounced in the 0–500 m SRH composites (Fig. 4). For both types of events, there is a local region of enhanced SRH in the immediate inflow region of the storm that is clearly higher than the SRH in the more distant, surrounding area. The difference of SRH in this enhanced region is  $\sim 200 \text{ m}^2 \text{ s}^{-2}$  greater in the tornadic than the nontornadic significant-hail supercells. The size of local regions of enhanced SRH is somewhat larger for the tornadic supercells. There also appears

to be a much sharper gradient in the composites of the SRH values that extend out from the center of the storm towards the east and south. These characteristics of enhanced SRH are interpreted as the average location of the leading edges of the forward- and rear-flanking downdrafts represented in WoFS. These features appear to be much better developed in WoFS for the cases that produced a tornado. Although the nontornadic significant-hail events tend to also have elevated SRH, their spatial extent is limited compared to tornado cases. The differences in spatial extent and magnitude are similar to the observed meso-beta-scale fields from Coniglio and Parker (2020), who find that the SRH is higher and broader in tornadic supercells than in nontornadic supercells. They suggest that higher SRH values well away from the updraft are at least partially from the background environment, but also that the tornadic supercells induce stronger perturbations such as a significantly stronger low-pressure perturbation in the meso-beta-scale area around the updraft.

Apart from the inflow region, interesting features are present in the PMM composites that occur west and southwest of the supercell. Higher CAPE exists in that region, but the high variability renders most of the difference insignificant. However, there are significant and substantially lower LCLs in this region as well as significantly higher SRH just west of the supercell. We can only make conjectures regarding these features, but we do acknowledge that these features may be related to findings in previous work highlighted in the introduction. In particular, cell mergers and boundary interactions can modify the near-storm environment and influence tornadogenesis (e.g., Lee et al. 2006; Fischer and Dahl 2023; Nixon et al. 2024). Given that our PMM composites from WoFS also reveal significant differences in these locations, it is at least consistent with those ideas. A different approach is necessary to reveal the underlying processes, but the existence of these features just west of the supercell may provide additional information since the supercells in WoFS that have this feature were associated with a reported tornado.

To examine the efficacy of established composite parameters to discriminate between events in the WoFS framework, the 500STP and SCP are examined in Fig. 5. Tornadic storms contain larger regions of relatively higher values of 500STP and SCP than their nontornadic significant-hail counterparts in the vicinity of the storms, but the most notable differences are near the storm within their inflow regions. When compared to the FSTP, which incorporates SRH from the 0-1 km layer (supplementary Fig. S16), the 500STP has roughly the same spatial distribution but has higher magnitudes than the FSTP, including larger differences between tornadic and

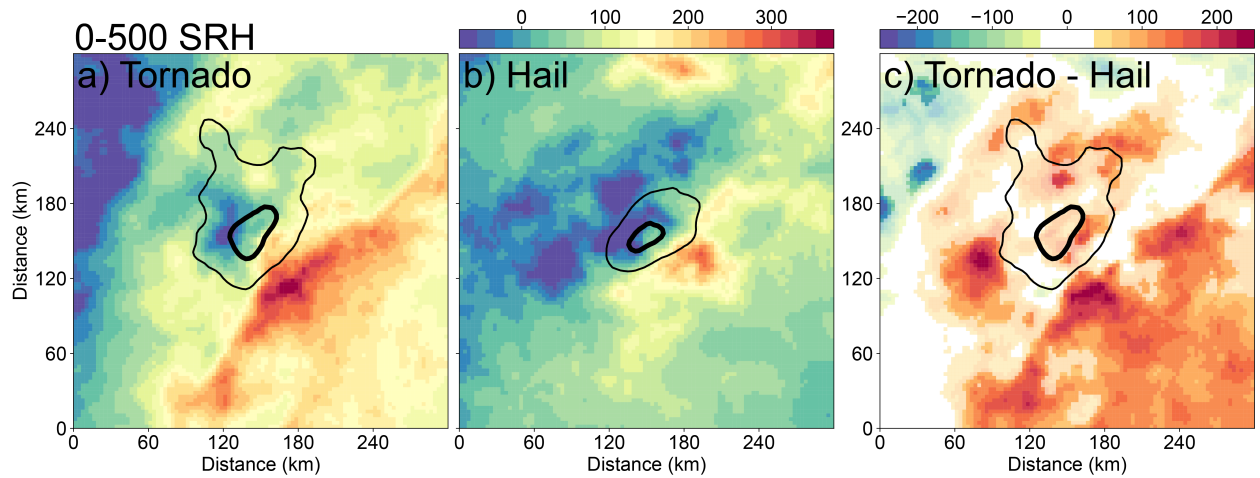


FIG. 4. As in Fig. 3, but for 0-500 m SRH ( $\text{m}^2 \text{s}^{-2}$ ).

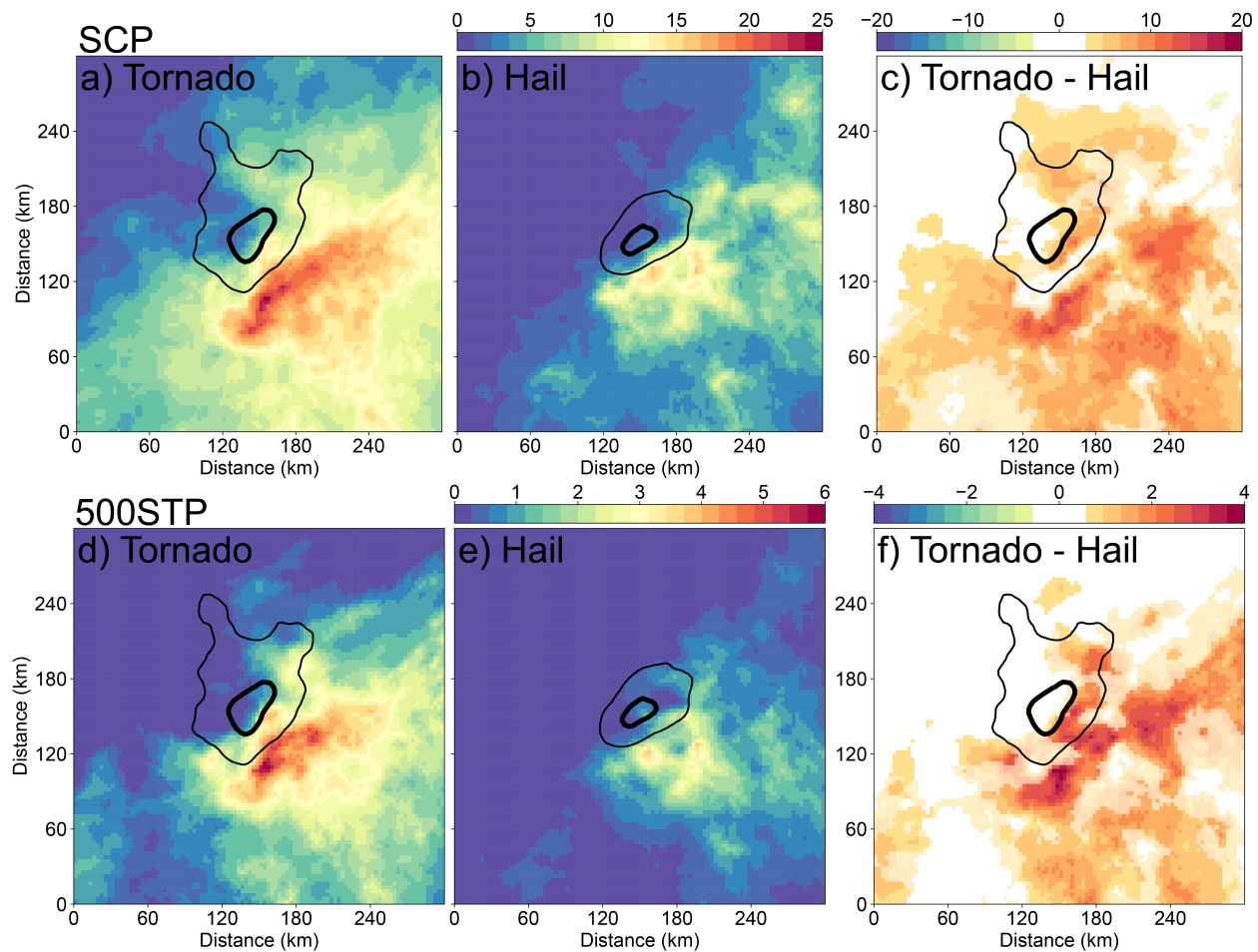


FIG. 5. As in Fig. 3, but for SCP and 500STP.

nontornadic significant-hail events. Lower-level SRH varied much more between event types than that of the 0-3 km layer that is typically more reflective of general mesocyclogenesis than tornadogenesis. However, larger differences in magnitude are actually noted in the SCP, which incorporates muCAPE and muCIN in lieu of the FSTP's selection of mixed-layer parcels.

## 2) ADDITIONAL PARAMETERS

Given the numerous parameters available to assess the convective environment (Table 1), this section provides an overview of their features and the additional figures are found in the supplemental material. Every available parameter was examined, and many indicated noticeable differences between tornadic and nontornadic significant-hail supercells. The CAPE and LCL of surface-based and mixed-layer parcels (Figs. S1-S4) are similar to those of most-unstable parcels shown in Figs. 3d-f. Since most of the reports observed in this study occurred in the late afternoon and early evening hours of late spring and early summer, the sbCAPE was often the same as the muCAPE. The mlCAPE values were  $\sim 500\text{-}1000 \text{ J kg}^{-1}$  lower than muCAPE and sbCAPE, which is similar to Bunkers et al. (2002), but all of the spatial structures were similar. Also, the LFC for all lifted parcel types (Figs. S8-S10) tends to be much more favorable (lower) in tornadic environments than nontornadic significant-hail environments with the supercells moving into areas of relatively lower LFCs.

Very little to no CIN is present for most-unstable nor surface-based parcels in the tornadic and nontornadic significant-hail spatial fields, especially close to the storms (Figs. S5-S7). Elevated values are only found associated with downdrafts and cold pools in the immediate wake of supercells for both event types. Mixed-layer parcels exhibit higher values of CIN within the regions that the storms are moving into with values near the storm of  $100\text{-}150 \text{ J kg}^{-1}$  in tornadic environments and  $150\text{-}200 \text{ J kg}^{-1}$  in nontornadic significant-hail environments<sup>1</sup>. The distributions shown later highlight that the high variability of CIN precludes any obvious threshold to discriminate between the two storm types. However, as will be noted in section 4b, even though there are little differences in the PMM, there are some differences in the distributions at earlier times (at least 30 min prior) with tornadic events containing a more pronounced tail towards higher muCIN values.

---

<sup>1</sup>WoFS became known for unusually large mlCIN values. NSSL updated the mlCIN calculation in 2023 to a method that gives values similar to other operational tools such as the Storm Prediction Center Mesoanalysis. The physical output of the ensemble in the vertical did not change, and spatial patterns in WoFS are therefore unaffected by this change.

The various wind shear metrics exhibit notable characteristics (Figs. S13-S15). The 0-1 km shear and 0-3 km shear are both much higher near tornadic supercells, especially within the immediate ~50 km of the storm itself. In contrast, the 0-6 km shear reveals only minor differences in the magnitude and spatial pattern between the tornadic and nontornadic significant-hail environments. The interactions between the deep-layer shear and updraft can produce pressure perturbation structures that are favorable for supercells in general but do little to determine if that supercell is tornadic or not (Markowski and Richardson 2010). Strength of the low-level shear is more strongly related to enhanced mesocyclogenesis with the lowest 0-1 km shear being a better indicator of tornadogenesis than the deep shear. Consequently, there is a notable difference between the low-level shear environments of the simulated convection occurring in WoFS associated with nontornadic significant-hail and tornado storm reports.

The SRH within the 0-1 km and 0-3 km layers (Figs. S11-S12) closely follows the spatial patterns of the 0-500 m layer, with differences mainly in magnitude. These differences in magnitude are also similar to the ones observed in the basic shear fields, as differences are more apparent in the layers closest to the ground and up to the 0-3 km layer. Elevated values of these fields are observed in close proximity to each storm, and these storms enter a broad region of elevated SRH as the time of each report approaches. The elevated values of low-level SRH shown in Fig. 4 are also seen in the 0-1 km and 0-3 km layers (especially in tornadic supercell environments) and maintain the same spatial patterns with higher magnitudes because they are over a deeper layer. As with the 0-500 m SRH, these deeper layer SRH fields in WoFS appear to discriminate between tornadic and significant-hail supercells. This suggests an underlying physical meaning, and just as importantly demonstrates that WoFS can capture meso-beta-scale features that are predictive of different outcomes.

### 3) SUMMARY OF COMPOSITES

Following earlier findings such as Craven and Brooks (2004), LCLs are broadly below 1500 m and are also noted to be generally lower in tornadic environments than in nontornadic significant-hail environments, with few cases being the exception. For all cases, the CAPE is in excess of 2000  $\text{J kg}^{-1}$  over a wide area, which is not surprising for severe weather events that are taken mostly from the Great Plains. In these cases, CAPE is generally higher in the tornadic environments, but only the

largest differences in CAPE are significant given that CAPE varies greatly from case to case. High CAPE is not a necessity for tornadic supercells since the dynamically driven accelerations will be large in high-shear, low-CAPE environments (Wade and Parker 2021). Climatological distributions of CAPE indicate some relationship between higher CAPE and larger hail, and there is considerable overlap in these distributions as well (Taszarek et al. 2020). However, the relationship of CAPE to large hail is not necessarily monotonic, and large hail depends on an optimal shear-CAPE relationship and can also be impacted by different vertical distributions of buoyancy that have the same CAPE (Lin and Kumjian 2022).

As expected, the most significant differences in WoFS occur when examining the kinematic fields such as the SRH. The output from WoFS depicts meso-beta pockets of elevated SRH that are enhanced well beyond the background levels and are frequently observed within the inflow region of tornadic and only a few nontornadic significant-hail supercells. These enhancements of SRH from the background values, often in excess of  $100 \text{ m}^2 \text{ s}^{-2}$ , are especially present in the 0-500 m and 0-1 km layers, though elevated values are also noted in the 0-3 km layer as well. Given that the 500STP incorporates several factors including low-level shear that favor tornadoes, the 500STP fields also exhibit differences between tornadic and nontornadic significant-hail supercells including an elevated pocket near the storm. Even with fewer components than the 500STP, the SCP depicts similar features to the 500STP with higher values in the tornadic events than for nontornadic significant-hail events.

### *b. Parameters along back trajectories*

#### 1) PRIMARY PARAMETERS

The muCAPE and muLCL (Fig. 6) reveal differences between the events that are similar to those in the composites (Fig. 3). muCAPE for an inflow parcel is generally higher for tornadic events at all times with mean differences of  $\sim 500 \text{ J kg}^{-1}$ . Both sets of events tend to exhibit a slight decrease of muCAPE as the parcels approach the convection at the time of the associated storm report, and the overlap of the interquartile range is the smallest an hour before the storm report. The mean height of the muLCL and its distribution for tornadic events remains nearly the same during the entire hour leading up to the event. For the nontornadic significant-hail supercells, the LCL is

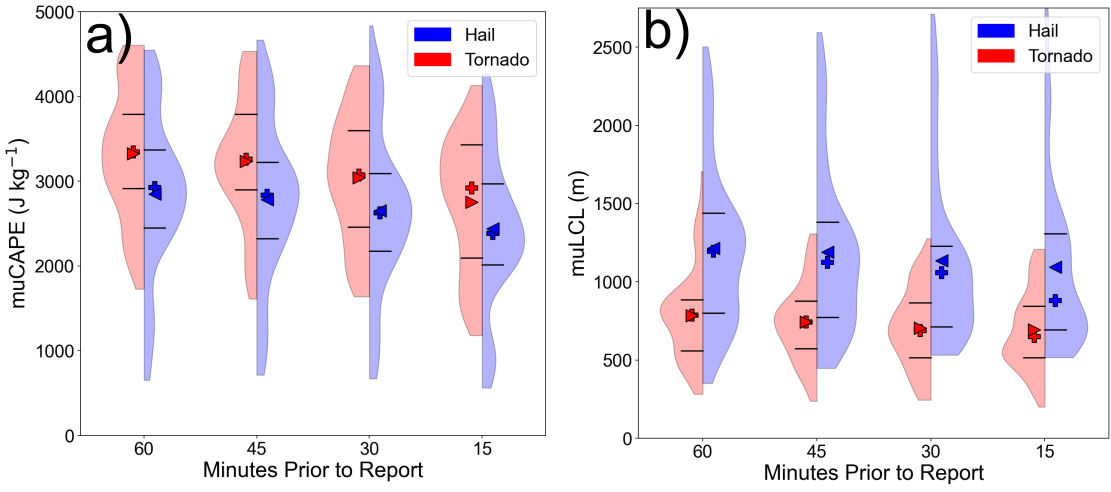


FIG. 6. Using the back trajectory method described in section 3b, the evolution of the (a) muCAPE ( $\text{J kg}^{-1}$ ) and (b) muLCL (m) for tornadic (red) and significant-hail (blue) events depicted by violin plots including the mean (triangle), median (plus), and the quartile range (horizontal lines). Differences that are not significant are indicated by a large X.

much higher ( $\sim 400$  m) and, unlike the tornadic supercells, there is a prominent tail towards higher heights in the distribution.

Although the PMM composites of muCIN, which are from 15-minutes prior to the event, show little difference between tornado and nontornadic significant-hail events (Figs. S5-S7), the back trajectories of muCIN (Fig. 7) reveal some differences in the distributions between the tornadic and nontornadic significant-hail supercells that also change over time. At 15 minutes prior to the event, the interquartile range of muCIN is similar between tornado and nontornadic significant-hail supercells with only a slightly higher median for tornado events, but this difference is not significant. For earlier times, the median muCIN for nontornadic significant-hail events is close to zero with a small interquartile range, but the distribution for tornadic supercells is skewed towards greater magnitudes of muCIN. Differences between sbCIN and mlCIN are not significantly different. This is consistent with Parker (2014) who found comparable values of sbCIN for tornadic and nontornadic supercells.

The 0-500 m SRH (Figs. 8a-b) indicates clear differences between tornadic and nontornadic significant-hail supercells with very little overlap in the interquartile range at all times. The difference between means is statistically significant for all times and is the greatest difference of all

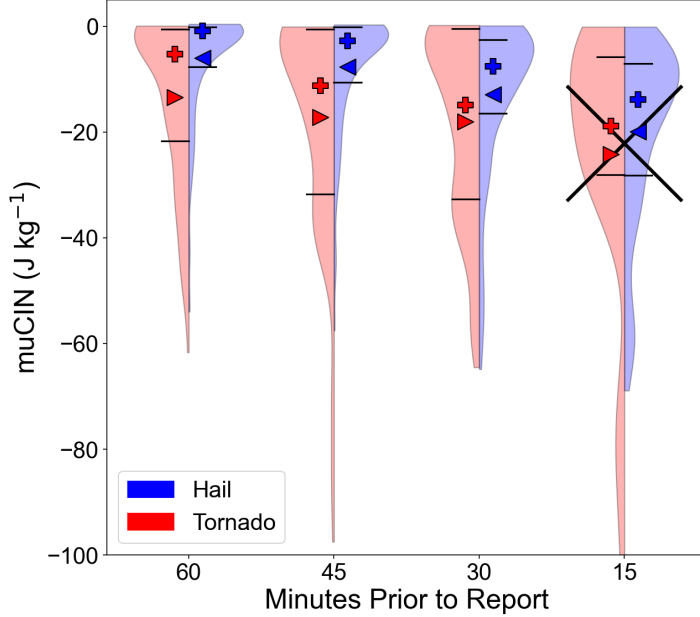


FIG. 7. As in Fig. 6, but for muCIN ( $\text{J kg}^{-1}$ ).

parameters examined. Both sets of cases have fairly clear increasing trends of the SRH as parcels approach the storm and the time of report, with tails of the distribution broadening in the last 15 minutes. The 0-3 km SRH (Fig. 8c-d) depicts similar features, but there is clearly more overlap. At an hour before the storm report, the differences are the greatest and diminish at each time step until there is considerable overlap just before the storm report occurred. This is consistent with the idea that the 0-3 km SRH is appropriate for predicting mesocyclogenesis, but the 0-500 m SRH is better for predicting tornadogenesis (Markowski and Richardson 2010; Coffer et al. 2019).

The SCP and 500STP (Fig. 9) attempt to simultaneously capture the influence of many factors that can contribute to developing a supercell or a tornado, respectively. They are constructed to discriminate better than any single parameter. The SCP shows elevated values for both event types with relatively broad distributions and some overlap between the two sets of cases. The SCP indicates that tornadic supercell environments on average had values that were about seven units higher than those of nontornadic significant-hail supercell environments. The 500STP interquartile ranges for the nontornadic significant-hail cases are fairly consistent over time, and there is just a slight increase in the mean that is mainly due to a broadening tail towards higher values. The tornadic supercells start with higher 500STPs an hour before the storm report, and the distributions

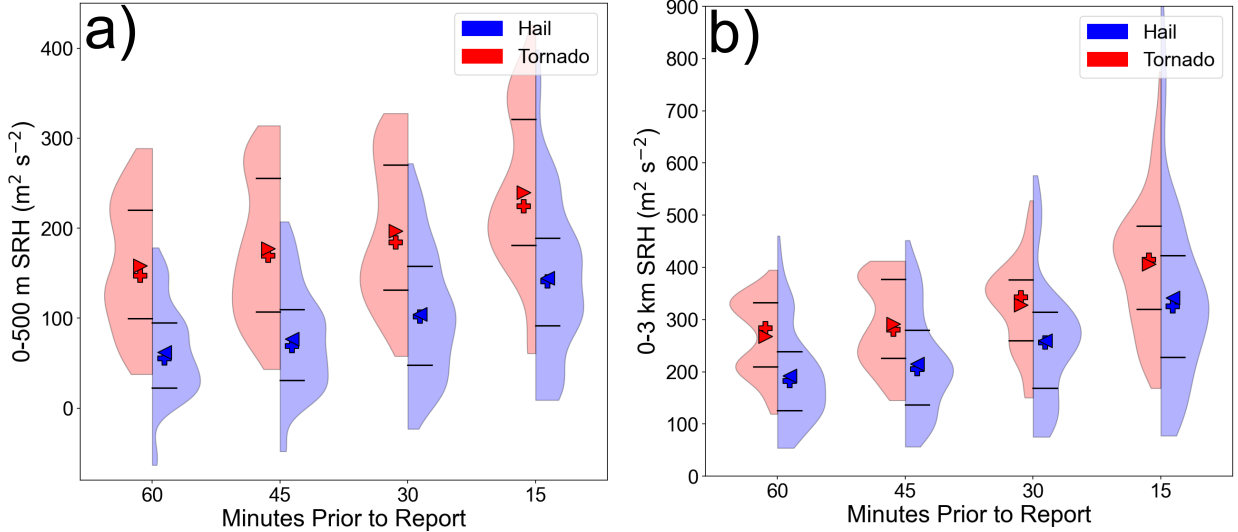


FIG. 8. As in Fig. 5, but for (a) 0-500 and (b) 0-3 km SRH ( $\text{m}^2 \text{s}^{-2}$ ).

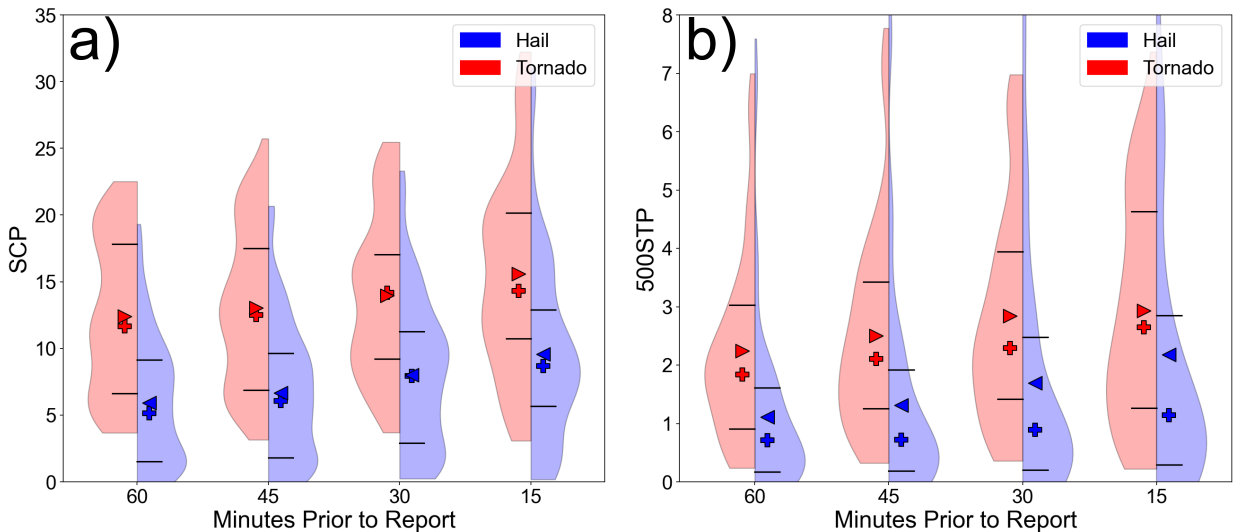


FIG. 9. As in Fig. 5, but for (a) SCP and (b) 500STP.

also broaden over time. The mean 500STPs of the tornado cases are at least 0.5 higher than the nontornadic significant-hail cases at all times. The overlap of the interquartile ranges seen in the 500STP slightly increases using the FSTP (Fig. S27).

## 2) ADDITIONAL PARAMETERS

The mixed-layer and surface-based CAPE and LCL display similar features in the trends leading up to the storm report (Figs. S17-S20). mlCAPE declines by about  $\sim 500 \text{ J kg}^{-1}$  in the hour

leading up to each storm report, while sbCAPE sees an even greater decrease of  $\sim 1000 \text{ J kg}^{-1}$  for tornadic cases. The differences in LCL between events remain relatively consistent, with the LCL  $\sim 400 \text{ m}$  lower for tornadic cases using both the mixed-layer and surface-based parcels. mLCL exhibits consistently lower values within both event spaces than the surface-based and most-unstable parcels, which have more similarities to each other in both temporal evolution and relative magnitude. All three lifted parcel types see an overall decrease in value as parcels travel closer to the storm.

The distributions of the LFC also contain some overlap between events using mixed-layer and surface-based parcels (Figs. S23-S25). Tornadic environments generally contain lower LFCs, and the greatest differences are associated with the most-unstable parcels, which have an LFC nearly 400 m lower than the nontornadic significant-hail environments throughout the entire hour leading up to the report.

Shear within all examined layers (Figs. S28-S30) exhibits the same increasing trend as parcels move closer to the storm for each event type. This rate of increase remains fairly uniform across the examined shear layers. The 0-6 km shear contains substantial overlap between the event types, and the mean of the tornadic events is only about 3 kts higher than the nontornadic significant-hail events during the hour preceding the storm report. This reveals the similarities of deep shear simulated in WoFS for events in both categories, but the shear in the lower layers is clearly a much better discriminator between event types. In the 0-3 km layer, the tornadic cases average 7 kts greater than in nontornadic significant-hail cases with less overlap than the 0-6 km shear. This speaks to the potential ability of WoFS to capture the differences of low-level shear in the environment that lead to observed tornadogenesis associated with the supercells simulated in WoFS.

Differences in the shear and SRH in the 0-1 km layer (Figs. S26 and S28) are both similar to the 0-500 m SRH (Fig. 8). Shear within the 0-1 km layer indicates that the tornadic environments are on average 10 kts greater than in nontornadic significant-hail environments at each 15-minute interval during the hour leading up to the storm report. This difference is even more striking because there is minimal, if any, overlap between the interquartile ranges. These features further complement what is seen in the spatial composites. Additionally, they suggest that even in the modest sample size of this study, WoFS is able to capture the low-level features necessary to discriminate between tornadic and nontornadic significant-hail environments associated with individual supercells.

### 3) SUMMARY OF BACK TRAJECTORIES

Examining environmental parameters along back trajectories revealed their magnitudes, tendencies, and distributions between tornadic and nontornadic significant-hail supercells in WoFS. By applying a bootstrap hypothesis test to their differences, most of the examined parameters are significantly different with exceptions such as the mlCAPE, sbCIN, and mlCIN. Although so many parameters are significantly different between categories, the thermodynamic parameters yield little in the way of actual discriminating power due to a considerable amount of overlap between event types found in all fields except for the muLCL. Although there is substantial overlap in muCIN, at least 30 minutes prior to the report there is a noticeable tail towards larger magnitudes of muCIN for tornadic supercells. Much more robust discriminating power becomes evident in the kinematic parameters of shear and SRH in the lower levels (e.g., 0-500 m and 0-1 km). These exhibit much smaller overlap between tornadic and nontornadic significant-hail supercells, and there are considerably higher values within tornadic environments than in nontornadic significant-hail environments. Not only do these results reflect the importance of low-level shear within tornadic environments (Coffer et al. 2019), they also exhibit minimal overlap in the interquartile ranges of event types and therefore suggest that they may serve as a prime indicator when using WoFS output.

## 5. Summary and Conclusions

The overall goal of this work is to support the community shift from a warn-on-detection to a warn-on-forecast paradigm. Simulations from WoFS are used because it is a state-of-the-art CAM ensemble that has a rapid update cadence. WoFS captures many of the processes pertaining to supercell development and the relevant near-storm environmental parameters on the meso-beta scale (Lawson et al. 2018). Although features such as tornadoes are not directly simulated, WoFS skillfully simulates environments containing severe weather (Snook et al. 2012, 2016; Yussouf et al. 2016; Flora et al. 2019; Britt et al. 2020; Potvin et al. 2020). This work seeks to advance the broader goal of the WoF project by characterizing and quantifying meso-beta-scale features and their evolution near simulated supercells that produced either significant hail or a tornado, as indicated by local storm reports, and to ultimately contribute to the goal of improving the lead-time and specificity of hazard information on the watch-to-warning scale (Heinselman et al. 2024).

The focus on summarizing the meso-beta-scale features of supercells simulated by WoFS is in contrast to performing a broader climatological study of these threats, such as using environmental conditions several hours before the event or averaging over a broader area, using coarser model or reanalysis grids, or using a single model realization instead of an ensemble.

After linking verified storm reports of tornadoes (EF1 and above) and significant hail (51 mm in diameter and above) to the nearby supercell in WoFS, two main analysis methods were applied to capture the spatial distributions of salient parameters (e.g., the LCL, SRH, and 500STP) and also their evolution leading up to the storm report. The PMM composites were constructed by centering on the rotating updraft to illustrate plan view fields. The PMM composites reveal the magnitude and spatial distribution of the parameters at the meso-beta scale near the supercells, and highlight the differences between tornadic and nontornadic significant-hail supercells. A sense of the evolution and distribution is provided by calculating back trajectories of a cluster of parcels starting near the inflow at the time of the report. Parameters were extracted at 5-min intervals along the back trajectory. The evolution of the distributions of the parameters provided excellent information on the environmental changes along the parcel paths and the distribution widths provided insight into the potential of a particular parameter to discriminate between tornadic and nontornadic significant-hail supercells. The main highlights from these two methods are:

- Tornadic supercells have a greater extent of the simulated reflectivity and a more concave shape of the 50 dBZ contour, which suggests counter-clockwise rotation indicative of a stronger rear-flank downdraft.
- CAPE of tornadic supercells was  $\sim$ 500-1000 J kg $^{-1}$  more within their inflow region than those of nontornadic significant-hail, but the broad distribution limits discriminating potential.
- LCLs associated with tornadic supercells were  $\sim$ 500-1000 m lower than nontornadic significant-hail supercells mainly in the southern half of the composite domain with a notably large difference west-southwest of the supercell. The distributions of LCL along the back trajectories reveal that the LCLs for tornadic supercells were much narrower and consistently low throughout the hour before the report.
- Both tornadic and nontornadic significant-hail supercell composites contained a well-defined meso-beta-scale pocket of enhanced 0-500 m SRH within their respective inflow regions,

but there were clear differences between tornadic supercells and nontornadic significant-hail supercells, which is consistent with Parker (2014).

- In the PMM composites, the local maximum of 0-500 m SRH for tornadic supercells approaches  $200 \text{ m}^2 \text{ s}^{-2}$  more than nontornadic significant-hail supercells and covers a greater spatial extent.
- In the back trajectories, the medians of 0-500 m SRH for tornadic supercells at all times were  $\sim 100 \text{ m}^2 \text{ s}^{-2}$  greater than nontornadic significant-hail supercells with little to no overlap in the interquartile range. Deeper layers of SRH exhibited smaller differences and more overlap.
- Consistent with their components, the SCP and 500STP also revealed differences between the tornadic and nontornadic significant-hail supercells with slightly sharper differences in the SCP.

Even with the modest sample size, many of the environmental parameters associated with tornadic or significant-hail supercells have differences that are statistically significant. For parameters such as 0-500 m SRH, the differences are statistically significant, substantial in magnitude, and have a small overlap. Because many of the other parameters contain considerable overlap, establishing a single threshold that firmly distinguishes between threat types remains elusive. However, other meso-beta-scale features such as the magnitude, spatial extent, and sharpness of the 0-500 SRH field in WoFS are worth noting.

Examining individual cases, the low-level wind shear and SRH exhibited notably elevated levels in the presence of most tornadic supercells and just a few of the nontornadic significant-hail supercells. Although these pockets of high values varied in magnitude and size, their recurring presence in WoFS output could be useful to help track supercells that are more likely to be associated with a tornado. Methods that only examine the broader environment may not detect these meso-beta features that occur in WoFS, and the existence of such a feature may provide a simple and quick visual diagnostic to help determine the likelihood that a tornado will be associated with a particular supercell simulated in WoFS.

These results indicate that WoFS contains clear differences between tornadic and nontornadic significant-hail supercells as defined by this study, which are also consistent with previous studies (Thompson et al. 2003; Coffer et al. 2019). Although the multiple component indices of STP and

SCP were built off of different datasets for different purposes, the differences between tornadic and nontornadic significant-hail supercells were substantial for both indices. Although the STP and SCP were not formulated based on WoFS output, they could be modified to better reflect the fields within the WoFS framework.

WoFS not only performs well and is consistent with previous work, but these results provide additional information regarding the model-derived differences between tornadic and nontornadic significant-hail supercells at the meso-beta spatial scale and during the hour leading up to the storm report. Despite these promising findings, some limitations must be taken into account. One such limitation regards WoFS' floating domain and relatively short historical archive when compared to other CAMs such as the High Resolution Rapid Refresh (HRRR), which decreased the number of eligible reports. The sample of storms collected for use in this research may not be entirely representative of the broader population of supercells modeled by WoFS. However, we think that this initial research establishes a solid baseline for what WoFS is able to model. Moreover, since each case was manually inspected, it is unlikely that any cases were misclassified, which can be an issue and a source of uncertainty for long-term climatologies that include many cases retrieved through an automated process.

*Acknowledgments.* Some of the computing for this project was performed at the OU Supercomputing Center for Education and Research (OSCER) at the University of Oklahoma (OU). We thank the reviewers for their constructive comments.

*Data availability statement.* WoFS data is available from the National Severe Storms Laboratory. Local Storm Reports are available from the National Centers for Environmental Information. All analysis code is available upon request.

## References

- Adlerman, E. J., and K. K. Droege, 2002: The sensitivity of numerically simulated cyclic mesocyclogenesis to variations in model physical and computational parameters. *Monthly Weather Review*, **130**.
- Anderson-Frey, A. K., and H. Brooks, 2019: Tornado fatalities: An environmental perspective. *Weather and Forecasting*, **34** (6), 1999 – 2015, <https://doi.org/10.1175/WAF-D-19-0119.1>.
- Benjamin, S. G., J. M. Brown, G. Brunet, P. Lynch, K. Saito, and T. W. Schlatter, 2019: 100 years of progress in forecasting and nwp applications. *Meteorological Monographs*, **59**, 13.1–13.67, <https://doi.org/10.1175/amsmonographs-d-18-0020.1>.
- Britt, K. C., P. S. Skinner, P. L. Heinselman, and K. H. Knopfmeier, 2020: Effects of horizontal grid spacing and inflow environment on forecasts of cyclic mesocyclogenesis in nssl's warn-on-forecast system (wofs). *Weather and Forecasting*, **35** (6), 2423–2444.
- Brooks, H., and C. Doswell, 1994: On the environments of tornadic and nontornadic mesocyclones. *Weather and Forecasting*, **9**, 606–618.
- Brooks, H. E., and J. Correia, 2018: Long-term performance metrics for national weather service tornado warnings. *Weather and Forecasting*, **33**, 1501–1511, <https://doi.org/10.1175/WAF-D-18-0120.1>.
- Bryan, G. H., J. C. Wyngaard, and J. M. Fritsch, 2003: Resolution requirements for the simulation of deep moist convection. *Monthly Weather Review*, **131**, 2394–2416.
- Bunkers, M. J., B. A. Klimowski, and J. W. Zeitler, 2002: The importance of parcel choice and the measure of vertical wind shear in evaluating the convective environment. *21st Conference*

*on Severe Local Storms*, San Antonio, TX, Amer. Meteor. Soc., P8.2, URL [https://ams.confex.com/ams/SLS\\_WAF\\_NWP/techprogram/paper\\_47319.htm](https://ams.confex.com/ams/SLS_WAF_NWP/techprogram/paper_47319.htm).

Burke, P. C., J. Barnwell, M. Reagan, M. A. Rose, T. J. G. Jr., R. Otto, and A. Orrison, 2024: The 21 august 2021 catastrophic flash flood at waverly, tennessee: Harnessing the warn-on-forecast system for confident pre-warning messaging of extreme rainfall. *Bulletin of the American Meteorological Society*, <https://doi.org/10.1175/BANS-D-23-0205.1>.

Burke, P. C., and Coauthors, 2022: Collaborating to increase warning lead time using the warn-on-forecast system. *30th Conference on Severe Local Storms*, Santa Fe, NM, Amer. Meteor. Soc., 44, <https://doi.org/https://ams.confex.com/ams/30SLS/meetingapp.cgi/Paper/407184>.

Coffer, B. E., M. D. Parker, R. L. Thompson, B. T. Smith, and R. E. Jewell, 2019: Using near-ground storm relative helicity in supercell tornado forecasting. *Monthly Weather Review*, **34**, 1417–1435, <https://doi.org/10.1175/WAF-D-19-0115.1>.

Coniglio, M. C., and M. D. Parker, 2020: Insights into supercells and their environments from three decades of targeted radiosonde observations. *Monthly Weather Review*, **148** (12), 4893–4915.

Coniglio, M. C., and R. L. Thompson, 2024: Impacts of sampling and storm-motion estimates on ruc/rap-based discriminations of nontornadic and tornadic supercell environments. *Weather and Forecasting*, **39** (10), 1417–1434.

Craven, J., and H. Brooks, 2004: Baseline climatology of sounding derived parameters associated with deep, moist convection. *National Weather Digest*, **28**, 13–24.

Davies-Jones, R., 2015: A review of supercell and tornado dynamics. *Atmospheric Research*, **158**, 274–291.

Davies-Jones, R. P., D. Burgess, and M. P. Foster, 1990: Test of helicity as a tornado forecast parameter. *Preprints, 16th Conference on Severe Local Storms*, 588 – 592.

Done, J., C. A. Davis, and M. Weisman, 2004: The next generation of nwp: Explicit forecasts of convection using the weather research and forecasting (wrf) model. *Atmospheric Science Letters*, **5**, 110–117, <https://doi.org/10.1002/asl.72>.

Dowell, D. C., and Coauthors, 2022: The high-resolution rapid refresh (hrrr): An hourly updating convection-allowing forecast model. part i: Motivation and system description. *Weather and Forecasting*, **37**, 1371–1395, <https://doi.org/10.1175/WAF-D-21-0151.1>.

Droegeemeier, K. K., S. M. Lazarus, and R. Davies-Jones, 1993: The influence of helicity on numerically simulated convective storms. *Monthly Weather Review*, **121** (7), 2005 – 2029, [https://doi.org/10.1175/1520-0493\(1993\)121<2005:TIOHON>2.0.CO;2](https://doi.org/10.1175/1520-0493(1993)121<2005:TIOHON>2.0.CO;2).

Ebert, E. E., 2001: Ability of a poor man's ensemble to predict the probability and distribution of precipitation. *Monthly Weather Review*, **129**, 2461–2480.

Fischer, J., and J. M. Dahl, 2023: Supercell-external storms and boundaries acting as catalysts for tornadogenesis. *Monthly Weather Review*, **151** (1), 23–38.

Fischer, J., J. M. L. Dahl, B. E. Coffer, J. L. Houser, P. M. Markowski, M. D. Parker, C. C. Weiss, and A. Schueth, 2024: Supercell tornadogenesis: Recent progress in our state of understanding. *Bulletin of the American Meteorological Society*, <https://doi.org/10.1175/BAMS-D-23-0031.1>.

Flora, M. L., C. K. Potvin, P. S. Skinner, S. Handler, and A. McGovern, 2021: Using machine learning to generate storm-scale probabilistic guidance of severe weather hazards in the warn-on-forecast system. *Monthly Weather Review*, **149** (5), 1535 – 1557, <https://doi.org/10.1175/MWR-D-20-0194.1>.

Flora, M. L., P. S. Skinner, C. K. Potvin, A. E. Reinhart, T. A. Jones, N. Yussouf, and K. H. Knopfmeier, 2019: Object-based verification of short-term, storm-scale probabilistic mesocyclone guidance from an experimental warn-on-forecast system. *Weather and Forecasting*, **34** (6), 1721–1739.

Frame, J., and P. Markowski, 2013: Dynamical influences of anvil shading on simulated supercell thunderstorms. *Monthly weather review*, **141** (8), 2802–2820.

Gensini, V. A., C. Converse, W. S. Ashley, and M. Taszarek, 2021: Machine learning classification of significant tornadoes and hail in the united states using era5 proximity soundings. *Weather and Forecasting*, **36** (6), 2143 – 2160, <https://doi.org/10.1175/WAF-D-21-0056.1>.

- Grams, J. S., R. L. Thompson, D. V. Snively, J. A. Prentice, G. M. Hodges, and L. J. Reames, 2012: A climatology and comparison of parameters for significant tornado events in the united states. *Weather and Forecasting*, **27**, 106–123, <https://doi.org/10.1175/WAF-D-11-00008.1>.
- Guerra, J. E., P. S. Skinner, A. Clark, M. Flora, B. Matilla, K. Knopfmeier, and A. E. Reinhart, 2022: Quantification of nssl warn-on-forecast system accuracy by storm age using object-based verification. *Weather and Forecasting*, **37**, 1973–1983, <https://doi.org/10.1175/WAF-D-22-0043.1>.
- Heinselman, P. L., and Coauthors, 2024: Warn-on-forecast system: From vision to reality. *Weather and Forecasting*, **39**, 75–95, <https://doi.org/10.1175/WAF-D-23-0147.1>.
- Johns, R. H., J. M. Davies, and P. W. Leftwich, 1993: *Some Wind and Instability Parameters Associated With Strong And Violent Tornadoes: 2. Variations in the Combinations of Wind And Instability Parameters*, 583–590. American Geophysical Union, <https://doi.org/10.1029/GM079p0583>.
- Jones, T. A., and Coauthors, 2020: Assimilation of goes-16 radiances and retrievals into the warn-on-forecast system. *Monthly Weather Review*, **148** (5), 1829 – 1859, <https://doi.org/10.1175/MWR-D-19-0379.1>.
- Kain, J. S., S. R. Dembek, S. J. Weiss, J. L. Case, J. J. Levit, and R. A. Sobash, 2010: Extracting unique information from high-resolution forecast models: Monitoring selected fields and phenomena every time step. *Weather and Forecasting*, **25**, 1536–1542, <https://doi.org/10.1175/2010WAF2222430.1>.
- Kerr, C. A., B. C. Matilla, Y. Wang, D. R. Stratman, T. A. Jones, and N. Yussouf, 2023: Results from a pseudo-real-time next-generation 1-km warn-on-forecast system prototype. *Weather and Forecasting*, **38** (2), 307–319.
- Kerr, C. A., P. S. Skinner, D. R. Stratman, B. C. Matilla, Y. Wang, and N. Yussouf, 2025: Limitations of short-term thunderstorm forecasts from convection-allowing models with 3-km horizontal grid spacing. *Weather and Forecasting*, **40** (1), 223–234.
- Lawson, J. R., J. S. Kain, N. Yussouf, D. C. Dowell, D. M. Wheatley, K. H. Knopfmeier, and T. A. Jones, 2018: Advancing from convection-allowing nwp to warn-on-forecast: Evidence of progress. *Weather and Forecasting*, **33**, 599–607, <https://doi.org/10.1175/waf-d-17-0145.1>.

- Lee, B. D., B. F. Jewett, and R. B. Wilhelmson, 2006: The 19 april 1996 illinois tornado outbreak. part ii: Cell mergers and associated tornado incidence. *Weather and forecasting*, **21** (4), 449–464.
- Lin, Y., and M. R. Kumjian, 2022: Influences of cape on hail production in simulated supercell storms. *Journal of the Atmospheric Sciences*, **79** (1), 179–204.
- Lindley, T. T., A. B. Zwink, R. R. Barnes, G. P. Murdoch, B. C. Ancell, P. C. Burke, and P. S. Skinner, 2023: Preliminary use of convection-allowing models in fire weather. *Journal of Operational Meteorology*, **11**, 72–81, <https://doi.org/10.15191/nwajom.2023.1106>.
- Markowski, P. M., 2024: A new pathway for tornadogenesis exposed by numerical simulations of supercells in turbulent environments. *Journal of the Atmospheric Sciences*, **81** (3), 481–518.
- Markowski, P. M., E. N. Rasmussen, J. M. Straka, and D. C. Dowell, 1998: Observations of low-level baroclinity generated by anvil shadows. *Monthly weather review*, **126** (11), 2942–2958.
- Markowski, P. M., and Y. Richardson, 2010: *Mesoscale Meteorology in the Midlatitudes*. Blackwell Publishing, 201-213 pp.
- Marshall, T. P., J. McDonald, and G. Forbes, 2004: The enhanced fujita (ef) scale. *Preprints, 22nd Conf. on Severe Local Storms, Hyannis, MA, Amer. Meteor. Soc. B*, Vol. 3.
- McGovern, A., R. J. Chase, M. Flora, D. J. Gagne, R. Lagerquist, C. K. Potvin, N. Snook, and E. Loken, 2023: A review of machine learning for convective weather. *Artificial Intelligence for the Earth Systems*, **2** (3), e220 077, <https://doi.org/10.1175/AIES-D-22-0077.1>.
- Miller, W. J., and Coauthors, 2022: Exploring the usefulness of downscaling free forecasts from the warn-on-forecast system. *Weather and Forecasting*, **37** (2), 181–203.
- Nixon, C. J., J. T. Allen, M. B. Wilson, M. J. Bunkers, and M. Taszarek, 2024: Cell mergers, boundary interactions, and convective systems in cases of significant tornadoes and hail. *Weather and Forecasting*, **39** (10), 1435–1458.
- Nowotarski, C. J., and P. M. Markowski, 2016: Modifications to the near-storm environment induced by simulated supercell thunderstorms. *Monthly Weather Review*, **144** (1), 273–293.

- Orf, L., R. Wilhelmson, B. Lee, C. Finley, and A. Houston, 2017: Evolution of a long-track violent tornado within a simulated supercell. *Bulletin of the American Meteorological Society*, **98** (1), 45–68, <https://doi.org/10.1175/BAMS-D-15-00073.1>.
- Parker, M. D., 2014: Composite vortex2 supercell environments from near-storm soundings. *Monthly Weather Review*, **142** (2), 508–529.
- Potvin, C. K., K. L. Elmore, and S. J. Weiss, 2010: Assessing the impacts of proximity sounding criteria on the climatology of significant tornado environments. *Weather and Forecasting*, **25**, 921–930, <https://doi.org/10.1175/2010WAF2222368.1>.
- Potvin, C. K., and M. L. Flora, 2015: Sensitivity of idealized supercell simulations to horizontal grid spacing: Implications for warn-on-forecast. *Monthly Weather Review*, **143** (8), 2998–3024.
- Potvin, C. K., and Coauthors, 2020: Assessing systematic impacts of pbl schemes on storm evolution in the noaa warn-on-forecast system. *Monthly Weather Review*, **148** (6), 2567–2590.
- Potvin, C. K., and Coauthors, 2022: An iterative storm segmentation and classification algorithm for convection-allowing models and gridded radar analyses. *Journal of Atmospheric and Oceanic Technology*, **39**, 999–1013, <https://doi.org/10.1175/JTECH-D-21-0141.1>.
- Schwartz, C. S., and R. A. Sobash, 2017: Generating probabilistic forecasts from convection-allowing ensembles using neighborhood approaches: A review and recommendations. *Monthly Weather Review*, **145**, 3397–3418, <https://doi.org/10.1175/MWR-D-16-0400.1>.
- Skamarock, W. C., and Coauthors, 2019: A description of the advanced research wrf version 4. *NCAR tech. note ncar/tn-556+ str*, **145**.
- Skinner, P. S., and Coauthors, 2018: Object-based verification of a prototype warn-on-forecast system. *Weather and Forecasting*, **33** (5), 1225–1250, <https://doi.org/10.1175/WAF-D-18-0020.1>.
- Smith, B. T., R. L. Thompson, J. S. Grams, C. Broyles, and H. E. Brooks, 2012: Convective modes for significant severe thunderstorms in the contiguous united states. part i: Storm classification and climatology. *Weather and Forecasting*, **27**, 1114–1135, <https://doi.org/10.1175/WAF-D-11-00115.1>.

Snook, N., Y. Jung, J. Brotzge, B. Putnam, and M. Xue, 2016: Prediction and ensemble forecast verification of hail in the supercell storms of 20 may 2013. *Weather and Forecasting*, **31**, 811–825, <https://doi.org/10.1175/WAF-D-15-0152.1>.

Snook, N., M. Xue, and Y. Jung, 2012: Ensemble probabilistic forecasts of a tornadic mesoscale convective system from ensemble kalman filter analyses using wsr-88d and casa radar data. *Monthly Weather Review*, **140**, 2126–2146, <https://doi.org/10.1175/MWR-D-11-00117.1>.

Stensrud, D. J., and Coauthors, 2009: Convective-scale warn-on-forecast system: A vision for 2020. *Bulletin of the American Meteorological Society*, **90**, 1487–1499, <https://doi.org/10.1175/2009BAMS2795.1>.

Stensrud, D. J., and Coauthors, 2013: Progress and challenges with warn-on-forecast. *Atmospheric Research*, **123**, 2–16, <https://doi.org/10.1016/j.atmosres.2012.04.004>.

Taszarek, M., J. T. Allen, T. Púčik, K. A. Hoogewind, and H. E. Brooks, 2020: Severe convective storms across europe and the united states. part ii: Era5 environments associated with lightning, large hail, severe wind, and tornadoes. *Journal of Climate*, **33** (23), 10 263–10 286.

Thompson, R., R. Edwards, and J. Hart, 2002: Evaluation and interpretation of the supercell composite and significant tornado parameters at the storm prediction center. n.p.

Thompson, R. L., R. Edwards, J. A. Hart, K. L. Elmore, and P. Markowski, 2003: Close proximity soundings within supercell environments obtained from the rapid update cycle. *Weather and Forecasting*.

Thompson, R. L., R. Edwards, and C. M. Mead, 2004: An update to the supercell composite and significant tornado parameters. *Preprints, 22nd Conf. on Severe Local Storms, Hyannis, MA, Amer. Meteor. Soc. P*, Vol. 8.

Thompson, R. L., C. M. Mead, and R. Edwards, 2007: Effective storm-relative helicity and bulk shear in supercell thunderstorm environments. *Weather and Forecasting*, **22** (1), 102 – 115, <https://doi.org/10.1175/WAF969.1>.

Thompson, R. L., B. T. Smith, J. S. Grams, A. R. Dean, and C. Broyles, 2010: Climatology of near-storm environments with convective modes for significant severe thunderstorms in the

contiguous united states. *Preprints*, 25th Conf. Severe Local Storms, Denver, CO, Amer. Meteor. Soc.

Thompson, R. L., B. T. Smith, J. S. Grams, A. R. Dean, and C. Broyles, 2012: Convective modes for significant severe thunderstorms in the contiguous united states. part ii: Supercell and qlcs tornado environments. *Weather and Forecasting*, **27** (5), 1136 – 1154, <https://doi.org/10.1175/WAF-D-11-00116.1>.

Wade, A. R., and M. D. Parker, 2021: Dynamics of simulated high-shear, low-cape supercells. *Journal of the Atmospheric Sciences*, **78** (5), 1389–1410.

Wheatley, D. M., K. H. Knopfmeier, T. A. Jones, and G. J. Creager, 2015: Storm-scale data assimilation and ensemble forecasting with the nssl experimental warn-on-forecast system. part i: Radar data experiments. *Weather and Forecasting*, **30** (6), 1795–1817.

Wilson, K. A., P. L. Heinselman, P. S. Skinner, J. J. Choate, and K. E. Klockow-McClain, 2019: Meteorologists' interpretations of storm-scale ensemble-based forecast guidance. *Weather, Climate, and Society*, **11**, 337–354, <https://doi.org/10.1175/WCAS-D-18-0084.1>.

Wilson, K. A., and Coauthors, 2023: The NOAA weather prediction center's use and evaluation of experimental warn-on-forecast system guidance. *Journal of Operational Meteorology*, **11** (7), 82–94, [https://doi.org/https://doi.org/10.15191/nwajom.2023.1107](https://doi.org/10.15191/nwajom.2023.1107).

Yussouf, N., J. S. Kain, and A. J. Clark, 2016: Short-term probabilistic forecasts of the 31 may 2013 oklahoma tornado and flash flood event using a continuous-update-cycle storm-scale ensemble system. *Weather and Forecasting*, **31**, 957–983, <https://doi.org/10.1175/WAF-D-15-0160.1>.